Pergamon

Int. J. Heat Mass Transfer. Vol. 37, No. 15, pp. 2211–2219, 1994

0017–9310/94 $7.00+0.00

0017–9310(94)E0058–3

The influence of vapor–liquid interactions on the liquid pressure drop in triangular microgrooves

H. B. MA, G. P. PETERSON† and X. J. LU
Department of Mechanical Engineering, Texas A&M University, College Station, TX 77843, U.S.A.

(*Received* 10 *November* 1993 *and in final form* 28 *January* 1994)

Abstract—Presented herein is a mathematical model of the liquid pressure drop occurring in triangular grooves. The model considers the interfacial shear stresses due to liquid–vapor frictional interaction, and a dimensionless vapor–liquid interface flow number, L_v, is introduced. Results are reported for channel angles ranging from 20 to 60°, contact angles from 0 to 60°, and dimensionless vapor–liquid interface flow numbers of 0, 0.25, 0.5, 0.75, and 1. These results indicate that the friction factor Reynolds number product is strongly dependent upon the channel angle, the contact angle, and the dimensionless vapor–liquid interface flow number. The predicted results agree well with the documented and available experimental data for the cases $L_v = 1$ and $L_v = 0$.

INTRODUCTION

SMALL OR "microgrooves" of various shapes and sizes have been employed in a wide variety of applications in the chemical process industry to enhance the heat transfer and promote the flow of liquid to surfaces where evaporation occurs and away from condensing surfaces. Because of the potential cost savings involved, numerous investigations have been conducted. The recent development of micro heat pipes for use in the thermal control of high power transistors, LSI and VLSI circuits, and avionics packages, however, has stimulated a renewed interest in the flow in these channels.

Over the past 10 years, several analytical and experimental investigations of the vapor–liquid behavior in micro heat pipes have been conducted. In the initial micro heat pipe model, the vapor–liquid interface velocity was assumed to be zero [1]. Although reasonably accurate predictions of the performance of micro heat pipes were obtained using this model, some error was introduced. Somewhat later, steady-state [2] and transient [3] models were developed for trapezoidal micro heat pipes approximately 1 mm in dia. Although these models considered the frictional vapor–liquid interaction on the liquid flow by incorporating the friction factor, f_1, they utilized the results obtained previously by Sparrow *et al.* [4], which indirectly assumed that the vapor–liquid interface velocity was zero. Again, while predicting the performance reasonably well, some error was introduced due to this assumption. This work was followed by a model that included terms to account for the interfacial and vapor shear stress [5]. In calculating the friction factor, however, this model again assumed no frictional vapor–liquid interaction on the liquid flow, due to the lack of a method for estimating the correct friction factor.

As early as 1964, Sparrow *et al.* [4] investigated the flow inside internally finned annular flow passages and obtained an analytical solution for the pressure drop in fully developed laminar flow. The results obtained were shown to be accurate for single-phase flow in a finned annular flow passage in which the velocity at the boundaries was zero. Sometime later, Ayyaswamy *et al.* [6] conducted an investigation of capillary flow with a free surface in triangular grooves and found the solution to the two-dimensional equations of motion for steady laminar flow in grooves using Galerkin methods, but the vapor–liquid interaction on the liquid flow was still neglected.

In the current investigation, the effect of the interfacial shear stresses caused by the liquid–vapor frictional interaction occurring for flow in triangular grooves is investigated to determine how these forces affect the liquid pressure drop.

ANALYSIS

If the capillary flow of an incompressible Newtonian fluid in a groove with fully developed laminar vapor flow over the upper surface similar to that illustrated in Fig. 1 is considered, it is clear that the flow

† Author to whom correspondence should be addressed.

NOMENCLATURE

a	coefficient defined by equation (12)	Re	Reynolds number
A	cross-sectional area [m^2]	u	velocity [m s^{-1}]
D_e	hydraulic diameter [m]	$\bar{U}$	average velocity [m s^{-1}]
f	frictional factor	u_f	velocity of free surface liquid [m s^{-1}]
Hp	dimensionless number defined by equation (13)	$\bar{u}_f$	average velocity of free surface liquid [m s^{-1}]
K	constant	u^*	dimensionless velocity
L_v	dimensionless vapor–liquid interface flow number	x	coordinate defined by equation (3)
		z	axial coordinate [m].
P	pressure [N m^{-2}]		
Q	volume flow rate [m^3 s^{-1}]	Greek symbols	
r	radial coordinate [m]	α	contact angle [°]
r_1	radius defined by equation (9) [m]	θ	angular coordinate [°]
r_2	radius defined by equation (10) [m]	ϕ	channel half angle [°]
r_{w1}	groove boundary length [m]	μ	viscosity [kg m^{-1} s^{-1}]
r_{w2}	groove boundary length [m]	ρ	density [kg m^{-3}].

velocity and behavior of the liquid surface will be strongly influenced by the vapor flow direction and velocity. Utilizing a cylindrical coordinate system with the axis coincident with the apex (O), and assuming two-dimensional, fully developed flow of the liquid can be expressed as:

$$\frac{1}{r}\frac{\partial}{\partial r}\left(r\frac{\partial u}{\partial r}\right)+\frac{1}{r^2}\frac{\partial^2 u}{\partial \theta^2}=\frac{1}{\mu}\frac{\mathrm{d}p}{\mathrm{d}z}, \tag{1}$$

where u is the axial velocity, z the corresponding axial coordinate, and p is the static pressure. The boundary conditions for this expression are as follows: at $\theta = 0$

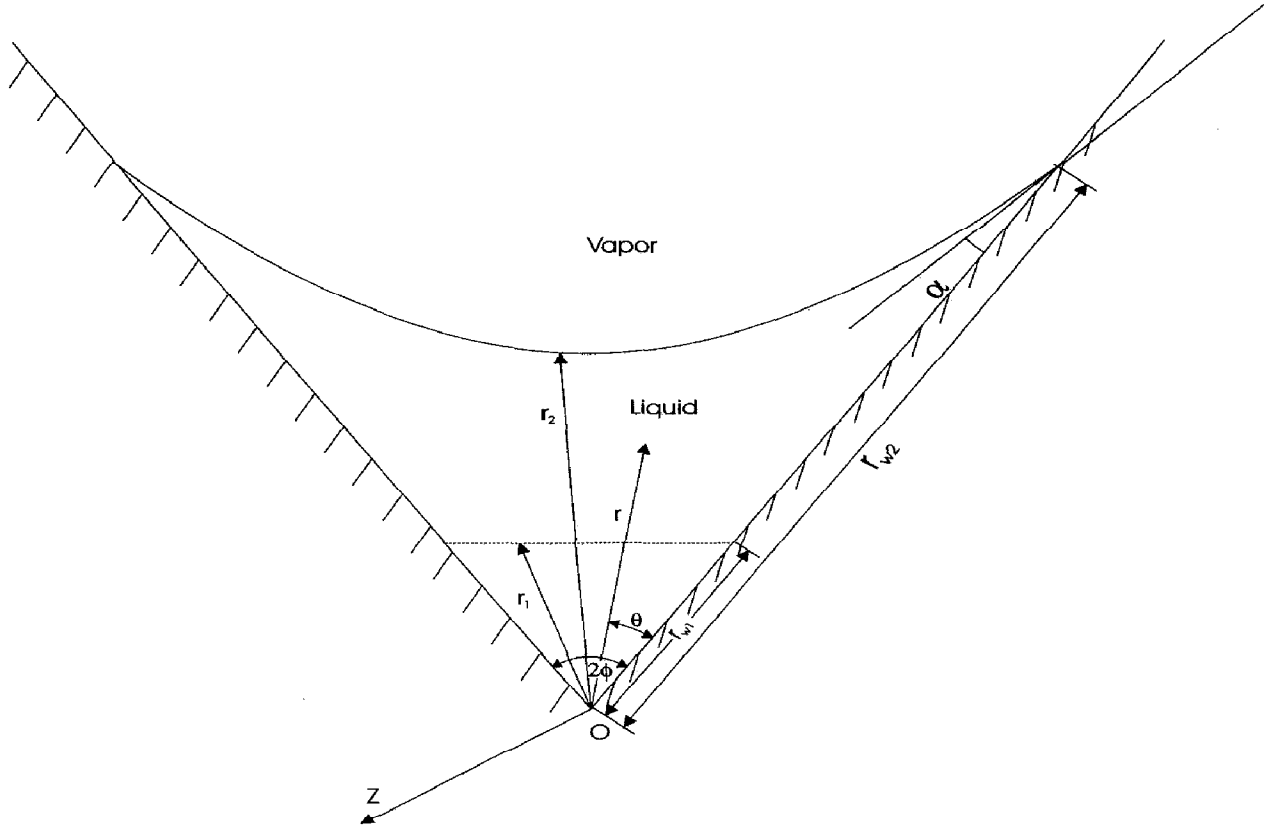

FIG. 1. Groove geometry and coordinate system.

and $\theta = 2\phi$, the velocity is equal to zero (i.e. a no slip condition at the wall is assumed); when $r = r_2$, the velocity of the liquid surface is equal to $\bar{u}_{r2}$. In order to obtain a general solution, a radius r_1 can be assumed. When $r = r_1$ the liquid velocity is equal to zero and, as $r_1 \to 0$, the solution corresponds to that obtained for a triangular groove, closed on all three sides. Applying a coordinate transformation:

$$u^* = \frac{u + r^2/4\mu(-\mathrm{d}p/\mathrm{d}z)}{\frac{r_1^2}{4\mu}(-\mathrm{d}p/\mathrm{d}z)}, \tag{2}$$

$$x = \ln\frac{r}{r_1}, \tag{3}$$

the governing equation and boundary conditions become, respectively:

$$\frac{\partial^2 u^*}{\partial x^2} + \frac{\partial^2 u^*}{\partial \theta^2} = 0, \tag{4}$$

$$u^* = \left(\frac{r}{r_1}\right)^2 = \mathrm{e}^{2x} \quad \text{at} \quad \theta = 0, \tag{5}$$

$$u^* = \left(\frac{r}{r_1}\right)^2 = \mathrm{e}^{2x} \quad \text{at} \quad \theta = 2\phi, \tag{6}$$

$$u^* = 1 \quad \text{at} \quad x = 0, \tag{7}$$

$$u^* = \frac{\bar{u}_{r2} + r_2^2/4\mu(-\mathrm{d}p/\mathrm{d}z)}{\left(\frac{r_1^2}{4\mu}\right)(-\mathrm{d}p/\mathrm{d}z)}$$

$$\text{at} \quad x = \ln\left(\frac{r_2}{r_1}\right). \tag{8}$$

For capillary flows at very low Bond numbers, the free surface will have a nearly constant radius of curvature, dependent upon the geometric shape of the liquid flow passage. The radii, r_1 and r_2, can be written as:

$$r_1 = r_{w1}\frac{\cos\phi}{\cos(\phi - \theta)}, \tag{9}$$

$$r_2 = r_{w2} \times \frac{\cos\alpha\cos(\phi-\theta) - [\sin^2\phi - \cos^2\alpha\sin^2(\phi-\theta)]^{0.5}}{\cos(\alpha+\phi)}. \tag{10}$$

Analytical and numerical methods

Equation (4) is a form of the Laplace equation where the exact solution is subject to the boundary conditions given in equations (5)–(8). The exact solution can be obtained utilizing a separation of variables method and linear superposition. The velocity u can be obtained as:

$$u = \frac{r_1^2}{4\mu}\left(-\frac{\mathrm{d}p}{\mathrm{d}z}\right)\left\{\frac{2}{\pi}\sum_{n=1}^{\infty}[1-(-1)^n]\frac{1}{n} \times \frac{\sinh\left[\frac{n\pi}{2\phi}(a-x)\right] + Hp\sinh\left(\frac{n\pi}{2\phi}x\right)}{\sinh\left(\frac{n\pi}{2\phi}a\right)} \times \sin\left(\frac{n\pi\theta}{2\phi}\right) + \frac{2}{\pi}\sum_{n=1}^{\infty} \times \frac{\frac{1}{n}\left[1-(-1)^n\left(\frac{r_2}{r_1}\right)^2\right]}{1+\left(\frac{2a}{n\pi}\right)^2} \times \frac{\sinh\left[\frac{n\pi}{a}(2\phi-\theta)\right] + \sinh\left(\frac{n\pi}{a}\theta\right)}{\sinh\left(\frac{n\pi}{a}2\phi\right)} \times \sin\left(\frac{n\pi}{a}x\right) - \left(\frac{r}{r_1}\right)^2\right\}, \tag{11}$$

where:

$$a = \ln\frac{r_2}{r_1}, \tag{12}$$

$$Hp = \frac{\bar{u}_{r_2} + r_2^2/4\mu(-\mathrm{d}p/\mathrm{d}z)}{\frac{r_1^2}{4\mu}(-\mathrm{d}p/\mathrm{d}z)}, \tag{13}$$

and the term, $\bar{u}_{r_2}$, in equation (13) represents the average velocity of liquid surface at $r = r_2$. This value depends not only on the flow characteristics and properties of the liquid, but also on the flow characteristics and properties of the vapor. It is quite difficult to obtain a general analytical solution for this term directly from the governing equations, since the flow of the liquid surface with the influences of vapor is not one-dimensional and therefore has an irregular cross-section.

To overcome these difficulties, the following analysis first assumes that the flow of the liquid surface is laminar, steady-state, and one-dimensional, and that the vapor–liquid frictional interaction has no effect on the liquid flow, i.e. the liquid surface is a free liquid surface without frictional influences. The momentum equation under these assumptions is

$$\mu\frac{\mathrm{d}^2 u_f}{r^2\,\mathrm{d}\theta^2} = \frac{\mathrm{d}p}{\mathrm{d}z}, \tag{14}$$

where u_f is the free liquid surface velocity without the influence of vapor shear stress and resulting friction. Utilizing the coordinate system shown in Fig. 2, the

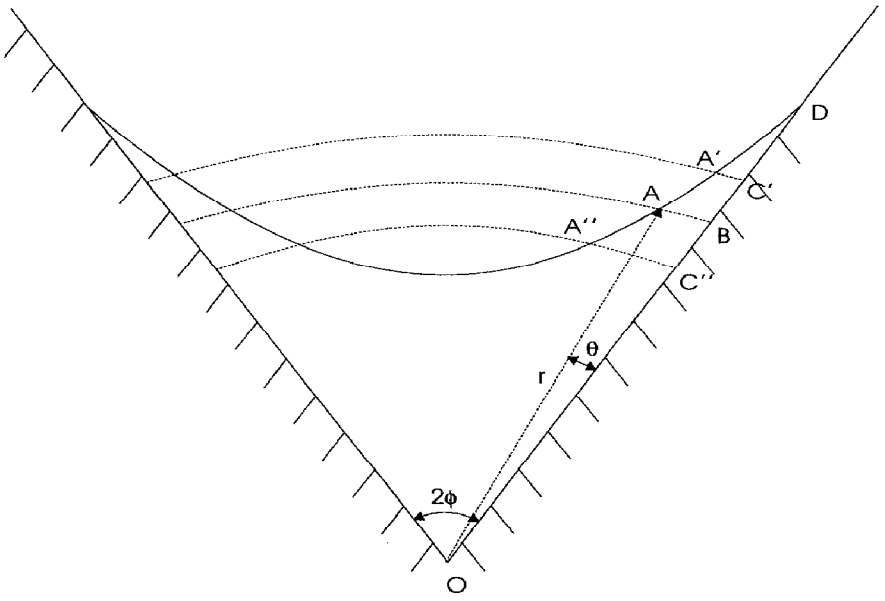

FIG. 2. Groove boundary influences on vapor–liquid interface.

boundary conditions corresponding to equation (14) are:

$$u_f = 0 \quad \text{at} \quad \theta = 0, \tag{15}$$

$$u_f = 0 \quad \text{at} \quad \theta = 2\phi. \tag{16}$$

The solution of equation (14) with these boundary conditions is:

$$u_f = \left(-\frac{1}{4\mu}\frac{dp}{dz}\right) \times \left[\frac{r_{w2}\{\cos\alpha\cos(\phi-\theta)-[\sin^2\phi-\cos^2\alpha\sin^2(\phi-\theta)]^{0.5}\}}{\cos(\alpha+\phi)}\right]^2 \times [4\phi\theta-2\theta^2]. \tag{17}$$

For convenience, especially in the actual case, the average velocity of the liquid flow usually is preferred. Taking the average as:

$$\bar{u}_f' = \frac{\int_0^{2\phi} u_f\,ds}{\int_0^{2\phi} d\theta}. \tag{18}$$

The average velocity of the free liquid surface with a one-dimensional assumption may be obtained as:

$$u_f' = \frac{1}{2\phi}\int_0^{2\Phi}\left(-\frac{1}{4\mu}\frac{dp}{dz}\right) \times \left(\frac{r_{w2}\{\cos\alpha\cos(\phi-\theta)-[\sin^2\phi-\cos^2\alpha\sin^2(\phi-\theta)]^{0.5}\}}{\cos(\alpha+\phi)}\right)^2 \times [4\phi\theta-2\theta^2]\,d\theta. \tag{19}$$

While the solution obtained above is for one-dimensional flow, in reality, the velocity of the free liquid surface (i.e. at point A) not only depends on the influence of point B, but also on the influence of points C, D, and the entire boundary along the solid surface from O to D. Since the one-dimensional assumption is not identical with the actual case, a coefficient K can be used to modify it. This coefficient, K, can be determined experimentally.

Utilizing the data of Ayyaswamy *et al.* [6], the coefficient K can be found to be equal to 0.52 for a 60° channel angle. To be precise, the coefficient K should vary with the channel apex angle θ. However, neglecting this effect and assuming K to be constant, results in a maximum error of 2.5% when compared with the available experimental data of Ayyaswamy *et al.* [6].

From the preceding discussion it is apparent that the actual velocity of the free liquid surface can actually be expressed as:

$$\bar{u}_f = K\bar{u}_f', \tag{20}$$

where $\bar{u}_f'$ is determined by equation (19).

Utilizing the actual average velocity of the liquid surface, a dimensionless vapor–liquid interface flow number, L_v, can be defined as:

$$L_v = \frac{\Delta\bar{u}}{\bar{u}_f}, \tag{21}$$

where:

$$\Delta\bar{u} = \bar{u}_f - \bar{u}_{r_2}, \tag{22}$$

and $\bar{u}_f$ is the average velocity of the free liquid surface obtained from equation (20). Substituting equation (21) into equation (22) results in an expression for the average velocity at r_2 of:

$$\bar{u}_{r_2} = \bar{u}_f(1-L_v). \tag{23}$$

Combining and substituting results in an expression for the average velocity, $\bar{u}_{r_2}$, of:

$$\bar{u}_{r_2} = \frac{K(1-L_v)}{2\phi}\int_0^{2\phi}\left(-\frac{1}{4\mu}\frac{dp}{dz}\right)$$

$$\times\left[\frac{r_{w2}\{\cos\alpha\cos(\phi-\theta)-[\sin^2\phi-\cos^2\alpha\sin^2(\phi-\theta)]^{0.5}\}}{\cos(\alpha+\phi)}\right]^2$$

$$\times[4\phi\theta-2\theta^2]\,d\theta. \quad (24)$$

From equation (24), it can be seen that the average velocity of the liquid surface is not only related to α, ϕ, θ, r_{w2}, and $(-dp/dz)$, but also to L_v. The physical meaning of the dimensionless vapor flow number, L_v, is as follows: when $L_v > 1$, the liquid velocity is parallel to the vapor velocity, but the flow directions are opposite. In this case, the relative vapor velocity has the largest value and as a result has the greatest influence on the liquid flow. The velocity distribution with vapor–liquid frictional interaction for this case is shown in Fig. 3a. When $L_v = 1$, as shown in Fig 3b, the liquid surface velocity is equal to zero, which can occur as a result of vapor–liquid frictional interactions or due to direct contact with a solid surface.

When $0 < L_v < 1$, as shown in Fig. 3c, the direction of the liquid flow is different from that of the vapor flow, and the velocity of the vapor is smaller than when $L_v \geqslant 1$ as shown in Fig. 3a and b. When $L_v = 0$, the liquid surface behaves as a free surface without any vapor–liquid interaction, as shown in Fig. 3d. And finally, when $L_v < 0$, the direction of the liquid flow is the same as that of vapor flow, as shown in Fig. 3e.

In actual applications, the value of L_v can be obtained utilizing the method presented by Lock [7], Potter [8], or Schlichting [9]. Once $\bar{u}_{r_2}$ is obtained, the velocity at any position (r, θ) can be found by numerical evaluation of equation (11). In addition, the volumetric flow-rate, Q, passing through any cross-section may be determined by integrating the velocity distribution:

$$Q = \int_0^{2\phi}\int_{r_1}^{r_2} ur\,dr\,d\theta = \left(-\frac{dp}{dz}\right)\frac{1}{4\mu}\int_0^{2\phi} r_1^4$$

$$\times\left[\sum_{n=1}^{\infty}\frac{2[1-(-1)^n]}{n\pi\left[1-\left(\frac{n\pi}{4\phi}\right)^2\right]\sinh\left(\frac{n\pi}{2\phi}a\right)}\right.$$

$$\times\left(-\frac{1}{2}\sinh\left(\frac{n\pi}{2\phi}a\right)+\frac{n\pi}{8\phi}\left[\left(\frac{r_2}{r_1}\right)^2-\cosh\left(\frac{n\pi}{2\phi}a\right)\right]\right.$$

$$+Hp\left\{\frac{1}{2}\left(\frac{r_2}{r_1}\right)^2\sinh\left(\frac{n\pi}{2\phi}a\right)-\frac{n\pi}{8\phi}\left[\left(\frac{r_2}{r_1}\right)^2\right.\right.$$

$$\left.\left.\left.\times\cosh\left(\frac{n\pi}{2\phi}a\right)-1\right]\right\}\right)\sin\left(\frac{n\pi\theta}{2\phi}\right)+\frac{1}{8}\left(\frac{n\pi}{a}\right)^2$$

$$\times\frac{1-(-1)^n\left(\frac{r_2}{r_1}\right)^2}{\left[1+\left(\frac{n\pi}{2a}\right)^2\right]^2}\frac{\sinh\left[\frac{n\pi}{a}(2\phi-\theta)\right]+\sinh\left(\frac{n\pi}{a}\theta\right)}{\sinh\left(\frac{n\pi}{a}2\phi\right)}\Bigg]\,d\theta$$

$$+\left(-\frac{dp}{dz}\frac{1}{4\mu}\right)\int_0^{\theta_1}\frac{r_1^4}{4}\left[1-\left(\frac{r_2}{r_1}\right)^4\right]d\theta. \quad (25)$$

The parameters a, r_2, r_1, and Hp included in equation (25) are determined from equations (9), (10), (12), and (13), respectively.

To this point, all of the techniques employed have been analytical. In evaluating equation (25), it is apparent that an exact analytical solution would be quite difficult to obtain: however, the coordinate transform utilized earlier changes the irregular cross-section of the liquid flow into a regular shape. Hence, a numerical difference method can be employed to solve this expression.

It is customary to define the friction factor as:

$$f = \frac{-dp/dz}{0.5\rho\bar{U}^2}\frac{D_e}{4} \quad (26)$$

in which $\bar{U} = Q/A$, and $D_e = 4A/p$, wherein A and P are the cross-sectional area and the wetted perimeter, respectively, and are equal to:

$$A = \frac{1}{2}\int_0^{2\phi}(r_2^2-r_1^2)\,d\theta, \quad (27)$$

$$P = 2r_{w2}. \quad (28)$$

The friction factor Reynolds number product, fRe, may be written as

$$fRe = \left(\frac{-dp/dz\ D_e}{2\rho\bar{U}^2}\right)\left(\frac{\rho\bar{U}D_e}{\mu}\right). \quad (29)$$

Figures 4–6 illustrate the relationship between the friction factor Reynolds product, fRe, and the contact angles, θ, as a function of the dimensionless vapor flow number, L_v. From these results, it is apparent that when L_v increases, the friction factor Reynolds number product increases. In addition for a given dimensionless vapor flow number, the friction factor Reynolds number product increases with increasing contact angle.

To verify the analytical model presented here, data from two previous investigations were compared with the values predicted by the model described above. The first of these was conducted by Sparrow *et al.* [4]. Their investigation is equivalent to $L_v = 1$, one of the special cases of the current study. When the same wetted perimeter and geometric shapes were evaluated, identical results were obtained.

For the second case, the values predicted by the present model were compared with both the experimental and analytical results obtained by Ayyaswamy *et al.* [6], where $L_v = 0$. The results of this

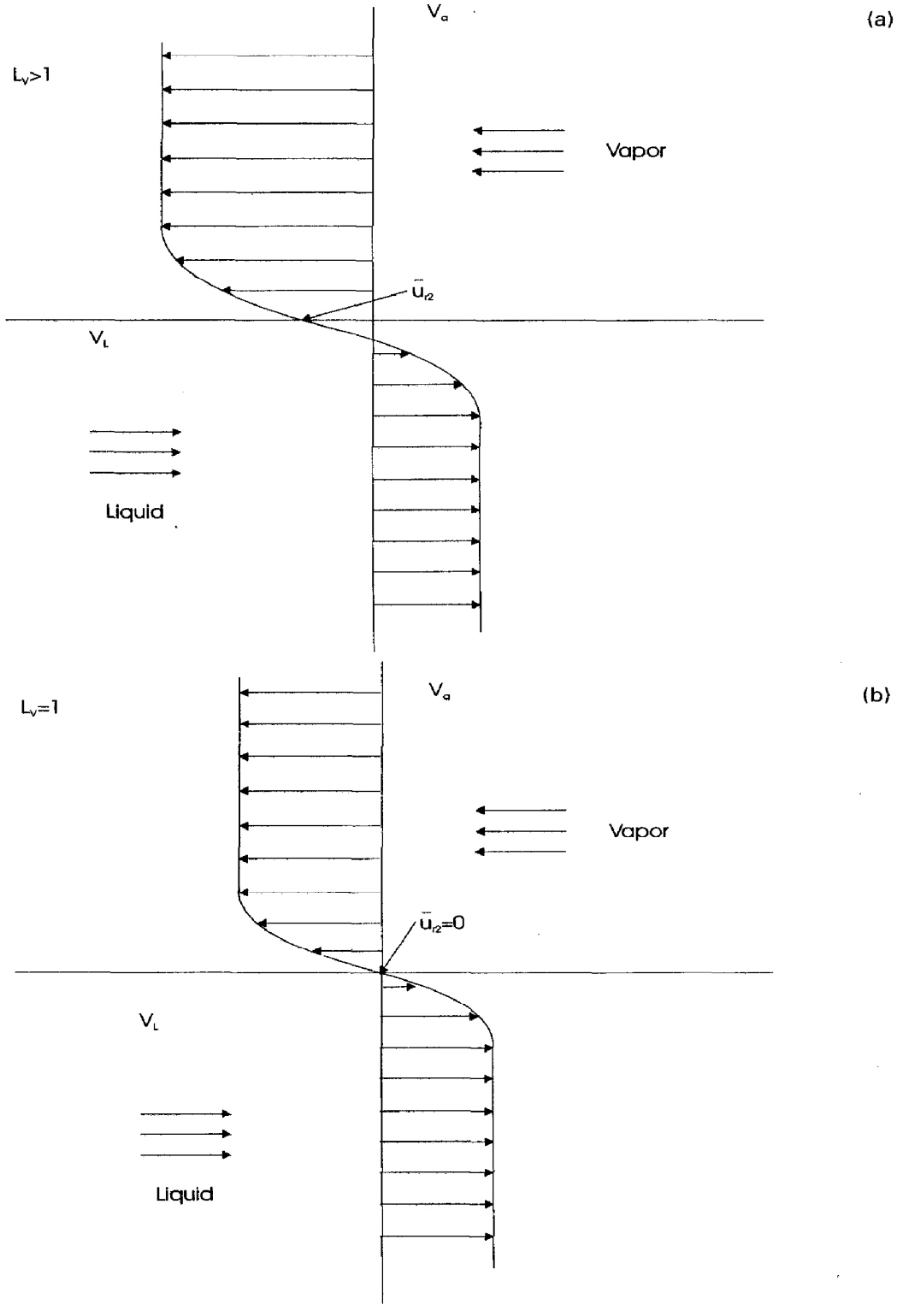

FIG. 3. (a) Vapor–liquid interaction at $L_v > 1$. (b) Vapor–liquid interaction at $L_v = 1$. (c) Vapor–liquid interaction at $1 > L_v > 0$. (d) Vapor–liquid interaction at $L_v = 0$. (e) Vapor–liquid interaction at $L_v < 0$.

comparison are illustrated in Figure 7. As shown, the correlation between the predicted and measured results is quite good at channel angles of 20°, 40°, and 60° for all contact angles. However, as the channel apex angle and contact angle increase, the error increases. At a channel apex angle of $2\phi = 60°$ and a contact angle of $\alpha = 60°$, the method described here results in a value of approximately 14.4. The analytical model of Ayyaswamy *et al.* results in a value of 13.8, and the experimental data yield a value of 14.2. This results in a variation between the prediction methods of approximately 4.3% and 1.4%.

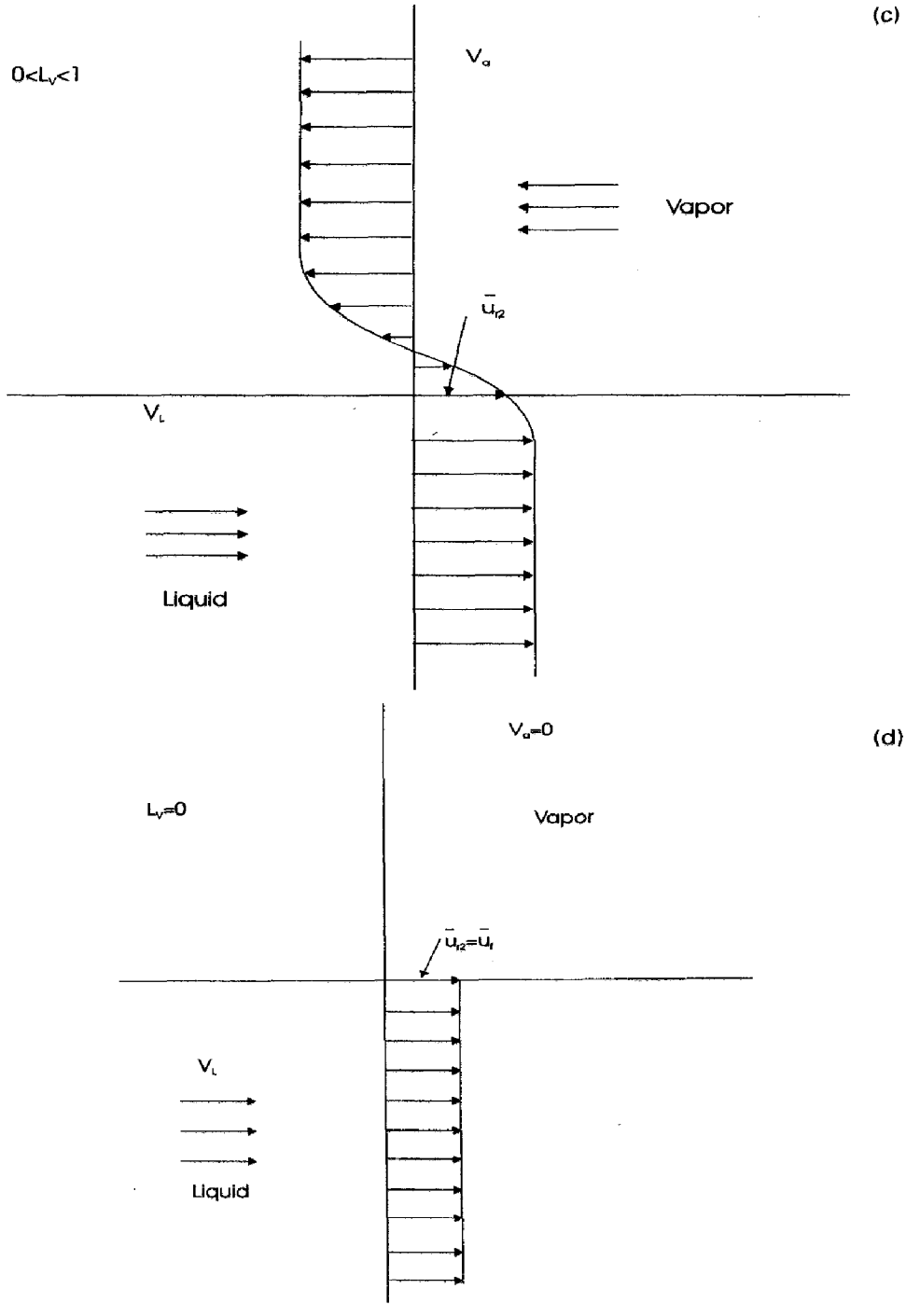

FIG. 3—*continued.*

CONCLUSIONS

A mathematical model of the liquid pressure drop occurring in triangular grooves with vapor flow occurring across a free surface, similar to the type occurring in the chemical processing industry or micro heat pipes was developed. The model considered the interfacial shear stresses and resulting frictional interaction at the liquid–vapor interface to determine how the direction and magnitude of the vapor flow influences the liquid flow. A dimensionless vapor–liquid interface flow number, L_v, was introduced to establish a relationship between the two flows.

The resulting model was solved using a combination of analytical and finite difference methods to overcome the difficulty resulting from the irregular cross-section. Results are reported for channel angles ranging from 20 to 60°, contact angles from 0 to 60°, and

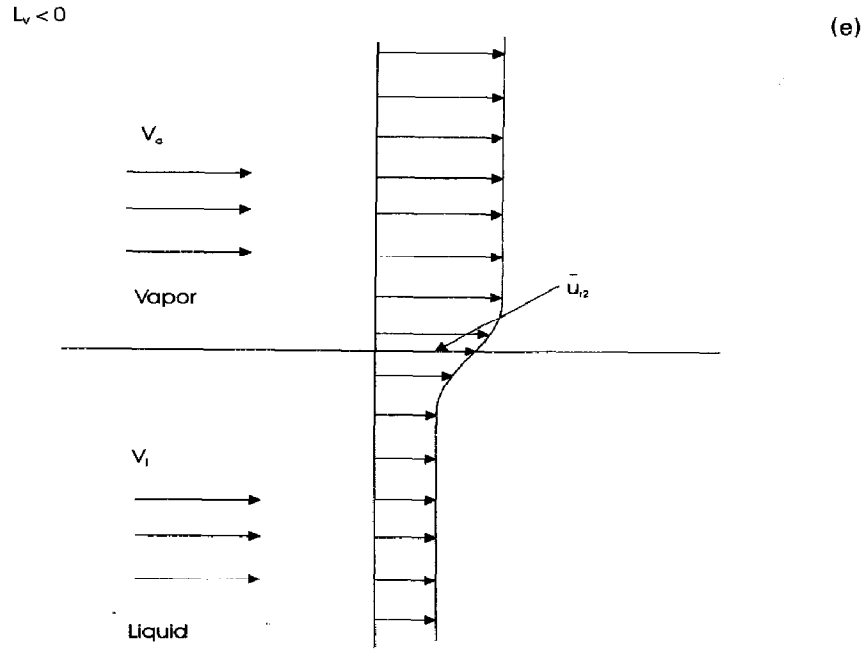

FIG. 3—*continued.*

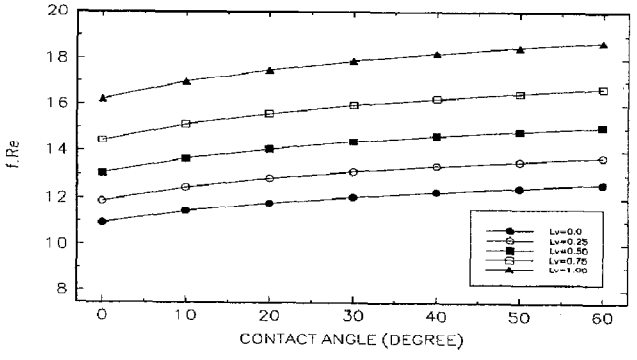

FIG. 4. Friction factor with contact angle at $2\phi = 20°$.

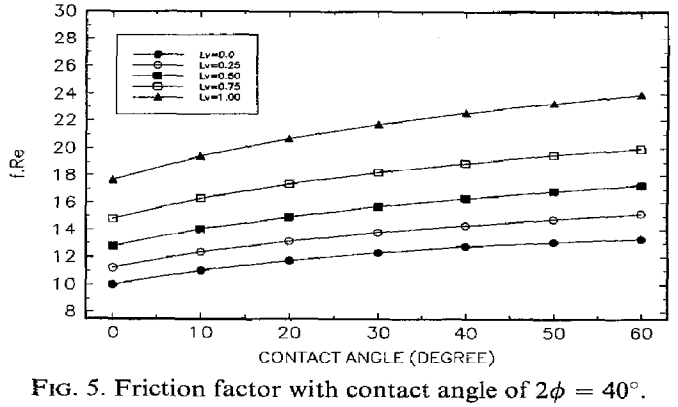

FIG. 5. Friction factor with contact angle of $2\phi = 40°$.

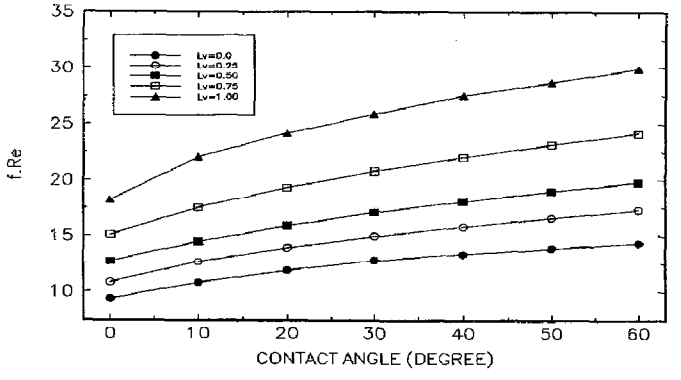

FIG. 6. Friction factor with contact angle of $2\phi = 60°$.

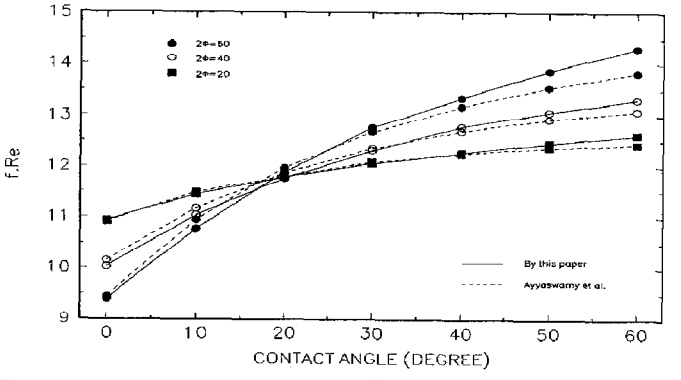

FIG. 7. Friction factor with contact angle for various groove angles at $L_v = 0$.

dimensionless vapor–liquid interface flow numbers of 0, 0.25, 0.5, 0.75, and 1. The results indicate that the friction factor Reynolds number product is strongly dependent upon the channel angle, the contact angle, and the dimensionless vapor–liquid interface flow number. Comparison of the predicted results with documented and available experimental data for cases of $L_v = 1$ and $L_v = 0$ were made and found to be in excellent agreement, with the largest variation occurring for the case of contact angles of 60° and apex angles of 60°.

REFERENCES

1. T. P. Cotter, Principles and prospects for micro heat pipes, *Proceedings of the 5th International Heat Pipe Conference*, Tskuba, Japan, pp. 328–335 (1984).
2. B. R. Babin, G. P. Peterson and D. Wu, Steady-state modeling and testing of a micro heat pipe, *ASME J. Heat Transfer* **112,** 595–601 (1990).
3. D. Wu and G. P. Peterson, Investigation of the transient characteristics of a micro heat pipe, *AIAA J. Thermophys. Heat Transfer* **5,** 129–134 (1991).
4. E. M. Sparrow, T. S. Chen and V. K. Jonsson, Laminar flow and pressure drop in internally finned annular ducts, *Int. J. Heat Mass Transfer* **7,** 583–585 (1964).
5. J. P. Longtin, B. Badran and F. M. Gerner, A one-dimensional model of a micro heat pipe during steady-state operation, *Proceedings of 8th International Heat Pipe Conference*, Beijing, China, c-5-1 to c-5-7 (1992).
6. P. S. Ayyaswamy, I. Catton and D. K. Edwards, Capillary flow in triangular grooves, *ASME J. Appl. Mech.* **41,** 332–336 (1974).
7. R. C. Lock, The velocity distribution in the laminar boundary layer between parallel streams, *Quart. J. Mech. Appl. Math.* **4,** 42–63 (1951).
8. O. E. Potter, Laminar boundary layers at the interface of co-current parallel streams, *Quart. J. Mech. Appl. Math.* **10,** 302–311 (1957).
9. H. Schlichting, *Boundary-Layer Theory*, pp. 182–185. McGraw-Hill, New York (1979).